

# CHAPTER III

## The Observed Stellar Mass Distribution and Gas Velocity Fields

Based on: “*K*-band Photometry and  $H\alpha$  Kinematics for Spiral Galaxies”  
Kranz & Rix, to be submitted to A&A (2002)

Many aspects of galactic research are closely related to the study of the galaxies’ stellar mass distributions and kinematics. The appearance of galaxies is rather dependent on the observed wavelength, and for different scientific purposes different spectral ranges are preferred to yield the desired information. To estimate the stellar mass content in galaxies, near infrared (NIR) wavebands are best suited since in the NIR dust absorption and population effects have the least effect on the surface brightness (e.g., Rix & Rieke 1993, Frogel et al. 1996). With the development of new infrared detector arrays that became operational mainly in the 90’s, objects can now be observed in the NIR with a resolution that compares to the one of CCD’s in visible wavelengths.

### 3.1. The galaxy sample

The need for obtaining a new data sample came from the specific requirements for this project. Since for the sample photometric as well as kinematic data are needed, there were some constraints which applied to the selection of candidates. First of all, the galaxies should be closeby and large enough to allow a fairly detailed sampling of their mass distribution. This requirement was met by considering only galaxies with an apparent diameter of  $> 2'$ . To reasonably resolve a their morphologies and to avoid extensive self absorption by gas and dust in the disk, for obtaining the photometry data galaxies with low inclinations with respect to the line-of-sight (LOS) would be preferred. However, the LOS component of the circular motion increases with inclination  $i$ , thus galaxies with low inclinations would be preferred. Due to the fact that the projection of the galaxy scales with  $\cos(i)$  and the LOS fraction of the velocity scales with  $\sin(i)$ , galaxies in the inclination range between  $\approx 30^\circ$  and  $\approx 60^\circ$  yield the most favorable conditions and were included in the sample.

In light of modelling the global gas dynamics in the galaxies, strong bars should be avoided because of their distinctly different dynamics from the rest of the disk. Still, strong spiral

## CHAPTER 3. OBSERVATIONS

**Table 3.1** Sample of galaxies observed in this project. For all galaxies NIR photometry is available. Kinematic data is available for a subsample of 8 galaxies.

Galaxy	$\alpha$ (2000) [hh mm ss.ss]	$\delta$ (2000) [dd mm ss.s]	Morph. type	$B_{\text{tot}}$ [mag]	velocity $\text{km s}^{-1}$	kin. data
NGC 2336	07 27 03.76	+80 10 39.6	SBc	13.46	+2200	
NGC 2339	07 08 20.66	+18 46 47.8	SBc	12.3	+2252	✓
NGC 2964	09 42 54.22	+31 50 48.5	Sb/Sc	12.0	+1328	✓
NGC 2985	09 50 22.20	+72 16 44.4	Sb	11.1	+1299	
NGC 3583	11 14 11.11	+48 19 04.6	SBb	11.6	+2098	
NGC 3810	11 40 58.88	+11 28 17.3	Sc	11.4	+958	✓
NGC 3893	11 48 38.43	+48 42 34.7	Sc	11.23	+972	✓
NGC 3953	11 53 49.08	+52 19 36.5	SBb	10.8	+1055	
NGC 4254	12 18 49.52	+14 25 00.4	Sc	10.2	+2453	✓
NGC 4321	12 22 54.95	+15 49 19.5	Sc	10.6	+1586	
NGC 4535	12 34 20.39	+08 11 51.3	SBc	11.1	+1962	
NGC 4653	12 43 50.89	-00 33 41.6	Sc	13.7	+2628	
NGC 5248	13 37 32.16	+08 53 05.9	Sbc	11.4	+1189	
NGC 5364	13 56 12.06	+05 00 52.8	Sc	13.2	+1267	✓
NGC 5371	13 55 39.97	+40 27 42.8	SBb	11.5	+2575	
NGC 5676	14 32 47.18	+49 27 28.6	Sc	11.7	+2114	✓
NGC 5985	15 39 36.77	+59 19 51.8	Sb	12.0	+2467	
NGC 6118	16 21 48.60	-02 17 02.8	Sc	13.2	+1574	
NGC 6643	18 19 46.58	+74 34 07.9	Sc	11.8	+1489	✓

Note: The data for the compilation of this Table are taken from the SIMBAD database, operated at CDS, Strasbourg, France

features are needed as the basis for the analysis. Thus, the sample was chosen to consist mainly of closeby, non-barred high luminosity galaxies with spiral arms that also appear strong in the NIR regime. Since all data were acquired at the Calar Alto observatory the last requirement is the visibility from southern Spain.

### 3.2. The data

First of all the NIR photometry was taken to determine, whether a galaxy was suited for this project, i.e. if its morphology shows strong and well defined spiral arms also in the NIR. The requirement for the kinematic measurements was to trace the gas velocity perturbations caused by the spiral arms, ideally across the whole disk. The two classical methods for obtaining 2D gas velocity fields are HI or CO radio observations and Fabry-Perot interferometry. Alternatively, longslit spectra taken at different position angles can be used to map the disk.

Single dish HI or CO observations are not suited for this project because they suffer from relatively bad angular resolution and poor sensitivity to faint emission between spiral arms

## 3.2. THE DATA

---

and the outer part of the disk. Sakamoto et al. (1999) recently published CO observations of a sample of spiral galaxies. In the velocity maps the signature of the spiral arms is in the majority of cases not or only barely visible. This most likely results from blurring the already weak velocity perturbations by beam smearing. 2D Fabry-Perot velocity fields provide the required angular resolution but usually give only a very patchy representation of the disk: Mainly the H II regions show up in the map (e.g., Weiner et al. 2001b). Because the coverage that can be achieved by taking eight longslit spectra across a galaxy's disk is reasonably high it was decided to collect the kinematic information by using a longslit spectrograph. Furthermore, this method yields good angular resolution and high sensitivity to faint H $\alpha$ -emission.

All observations were done with the 3.5 m telescope of the Calar Alto observatory in southern Spain. The Omega Prime camera with the  $K'$ -filter was used to acquire the NIR photometry and the TWIN longslit spectrograph was used to obtain the gas kinematics from the H $\alpha$  emission line.

### 3.2.1. NIR photometry observations

The Omega Prime infrared camera (Bizenberger et al. 1998) is located at the prime focus of the 3.5 m telescope. The detector is a  $1024 \times 1024$  pixel HgCdTe (1–2.5  $\mu\text{m}$ ) array made by Rockwell. The image scale is  $0''.3961$  per pixel, resulting in a field-of-view of  $6''.76 \times 6''.76$ . With this relatively large field-of-view, almost all galaxies fitted well on the detector, superseding the need for mosaicking.

The NIR photometric observations were carried out in 5 nights during two observing runs: 25. – 26. May 1999 and 16. – 18. March 2000. The weather conditions during the first run were only moderate, thus only a small part of the collected data was actually used later on. The March 2000 run had good conditions, although the seeing was not optimal ( $\sim 1''.4$  in  $K'$ ). The final sample consisted of 19 galaxies with good photometry that could be used to choose the candidates for the kinematic measurements. The sample is displayed in Figure 3.1.

At the first run the “Double Correlated Read” (dcr) readout mode was used for the array. The array is read immediately after the initial reset and again just before the final reset at the end of the integration. While one readout takes about 0.8 s for Omega-Prime, it has an enormous fraction of the telescope time, if one considers that a single integration time takes 2 to 3 s, and two readouts are needed per frame. For the second run a new readout mode was available, the “Full MPIA Mode” (rrr-fmpia). The new Full MPIA mode is “line oriented”. It reads out single lines while the whole array is integrating, leaving virtually no overhead time for the readout. This reduces the telescope time needed to effectively integrate 20 minutes on target by about 15 minutes to lie in the order of  $\sim 80$  minutes, including sky background observations and telescope slewing. The use of the “Full MPIA Mode” is highly encouraged!

Since the objects fill the complete array, a separate closeby background position was observed alternately with the galaxy to allow for sky background correction. The observing sequence was chosen to look like: G G – B B – G G – B B – . . . (G = galaxy, B = background position), taking two exposures of 30 s at each position. Any of these exposures is a stack of either 15 2-second exposures or 10 3-second exposures, depending on the atmospheric

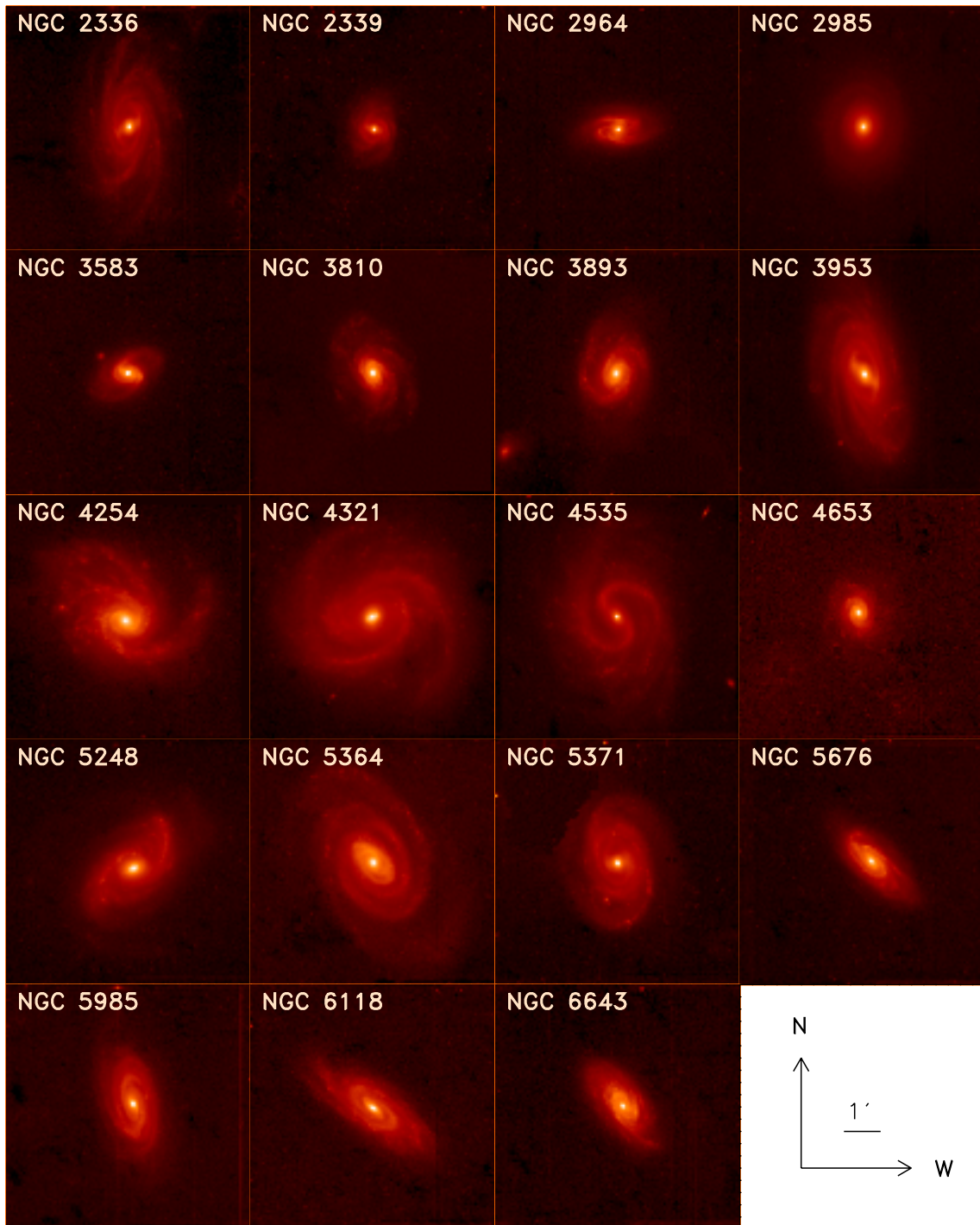


**Figure 3.1**  $K'$ -band ( $2.2\ \mu\text{m}$ ) images of all observed galaxies. For the images the entire field of view of the Omega Prime camera ( $6.76 \times 6.76$ ) is displayed. Bright foreground stars are masked out in all frames.

### 3.2. THE DATA

**Table 3.2** Observing log for the NIR photometry.

Galaxy	exposure [s]	seeing [" FWHM]	date [mm/yy]
NGC 2336	1260	1.14 ± 0.02	Mar 2000
NGC 2339	1200	1.05 ± 0.02	Mar 2000
NGC 2964	1260	1.18 ± 0.04	Mar 2000
NGC 2985	1260	1.13 ± 0.02	Mar 2000
NGC 3583	1260	1.24 ± 0.04	Mar 2000
NGC 3810	1200	1.11 ± 0.02	Mar 2000
NGC 3893	1320	1.16 ± 0.03	Mar 2000
NGC 3953	1800	1.15 ± 0.03	Mar 2000
NGC 4254	1350	1.74 ± 0.05	May '99, Mar '00
NGC 4321	1260	1.96 ± 0.04	Mar 2000
NGC 4535	1440	1.24 ± 0.03	Mar 2000
NGC 4653	1500	1.42 ± 0.04	Mar 2000
NGC 5248	1260	1.28 ± 0.04	Mar 2000
NGC 5364	2130	1.63 ± 0.05	Mar 2000
NGC 5371	1500	1.71 ± 0.03	Mar 2000
NGC 5676	2340	1.47 ± 0.03	May '99, Mar '00
NGC 5985	1260	1.56 ± 0.03	Mar 2000
NGC 6118	1440	1.39 ± 0.04	Mar 2000
NGC 6643	1860	1.44 ± 0.01	May '99, Mar '00

conditions. To perform two exposures of 30 s each instead of one with one minute exposure time was motivated to allow flexibility during short time weather changes. To account for stars at the background position, some dithering was introduced to enable a later removal of the stars. For calibration purposes, several standard stars from the Persson et al. (1998) sample were observed during the night. The final sample of the 19 galaxies with good  $K'$ -band photometry is given in Table 3.2.

#### 3.2.2. $H\alpha$ spectroscopy observations

The gas kinematics were measured from the  $H\alpha$  emission line. The data were taken during three observing runs with a total of about 10 nights at the 3.5 m telescope: 7. – 10. June 1999 (4 nights), 5. – 8. May 2000 ( $4 \times 0.8$  nights) and 2. – 7. December 2000 ( $6 \times 0.5$  nights). One more observing run was granted in February/March 2001, but no data could be attained due to bad weather. Finally, kinematic data for eight galaxies was collected, while for three of them the data set could not be completed.

The TWIN is a two channel longslit spectrograph, located at the cassegrain focus of the 3.5 m telescope. The data for this project were taken in the red channel, centered at the wavelength around the  $H\alpha$  line. The slit of the TWIN was set to measure  $4' \times 1''5$  on the sky. With the setup used, the TWIN achieved a spectral resolution of  $0.54 \text{ \AA}$  per detector pixel, which translates to  $24.8 \text{ km s}^{-1}$  LOS-velocity resolution per pixel. The

CHAPTER 3. OBSERVATIONS

**Table 3.3** Observing log for the H $\alpha$  spectroscopy.

Galaxy	NGC 2339							taken Dec 2000	
Slit position	13 $^{\circ}$ :1	33 $^{\circ}$ :4	57 $^{\circ}$ :5	85 $^{\circ}$ :0	112 $^{\circ}$ :6	136 $^{\circ}$ :6	157 $^{\circ}$ :0	175 $^{\circ}$ :0	
Integration time	1200s	1200s	1200s	1200s	1200s	1200s	1200s	1200s	
Galaxy	NGC 2964							taken Dec 2000	
Slit position	5 $^{\circ}$ :0	43 $^{\circ}$ :0	67 $^{\circ}$ :0	82 $^{\circ}$ :3	95 $^{\circ}$ :0	107 $^{\circ}$ :4	123 $^{\circ}$ :0	147 $^{\circ}$ :0	
Integration time	1200s	1200s	1200s	1200s	1200s	1200s	1200s	1200s	
Galaxy	NGC 3810							taken May 2000	
Slit position	15 $^{\circ}$ :0	30 $^{\circ}$ :5	49 $^{\circ}$ :0	73 $^{\circ}$ :2	105 $^{\circ}$ :0	136 $^{\circ}$ :8	161 $^{\circ}$ :2	179 $^{\circ}$ :5	
Integration time	1200s	1200s	1200s	1200s	1500s	1200s	1200s	$\approx$ 400s	
Galaxy	NGC 3893							taken Dec 2000	
Slit position	4 $^{\circ}$ :4	25 $^{\circ}$ :5	49 $^{\circ}$ :0	75 $^{\circ}$ :0	101 $^{\circ}$ :0	125 $^{\circ}$ :0	145 $^{\circ}$ :8	165 $^{\circ}$ :0	
Integration time	1200s	1200s	1200s	1200s	1200s	1200s	1200s	1200s	
Galaxy	NGC 4254							taken Jun 1999	
Slit position	0 $^{\circ}$ :0	22 $^{\circ}$ :5	45 $^{\circ}$ :0	67 $^{\circ}$ :5	90 $^{\circ}$ :0	112 $^{\circ}$ :5	135 $^{\circ}$ :0	157 $^{\circ}$ :5	
Integration time	1800s	1800s	930s	900s	900s	1200s	1200s	900s	
Galaxy	NGC 5364							taken May 2000	
Slit position	14 $^{\circ}$ :2	30 $^{\circ}$ :0	45 $^{\circ}$ :8	64 $^{\circ}$ :3	88 $^{\circ}$ :8				
Integration time	1200s	1200s	900s	1800s	2300s				
Galaxy	NGC 5676							taken Jun 1999	
Slit position	0 $^{\circ}$ :0	22 $^{\circ}$ :5	45 $^{\circ}$ :0	67 $^{\circ}$ :5	90 $^{\circ}$ :0	112 $^{\circ}$ :5	135 $^{\circ}$ :0	157 $^{\circ}$ :5	
Integration time	–	2400s	900s	1200s	1200s	1200s	1200s	1000s	
Galaxy	NGC 6643							taken Jun 1999	
Slit position	0 $^{\circ}$ :0	22 $^{\circ}$ :5	45 $^{\circ}$ :0	67 $^{\circ}$ :5	90 $^{\circ}$ :0	112 $^{\circ}$ :5	135 $^{\circ}$ :0	157 $^{\circ}$ :5	
Integration time	–	1000s	1200s	1200s	1200s	1000s	1000s	1000s	

spatial resolution of the CCD was reduced by a factor of two to increase the spectrograph's sensitivity to faint emission. It sampled the rotation curves of the galaxies with a resolution of  $1''.12$ , which is in accordance with the average seeing conditions. For each galaxy eight slit positions were planned to be taken across the disk to sample the 2D velocity field reasonably well. The angular separation of the different slit positions was chosen to  $22^{\circ}.5$  for the June 1999 observations. For later runs the sampling was chosen to provide an equidistant spacing in the deprojected reference frame of the galaxy. For that purpose an assumption for the major axis position angle and the inclination of the galaxy was made. The orientation of the slit positions and their individual exposure times are listed in Table 3.3 and is displayed in Figure 3.2 together with the reduced rotation curves along all taken slit positions. After each exposure a comparison exposure of a He-Ar arclamp was taken to constantly monitor the wavelength solution of the spectrograph.

### 3.2. THE DATA

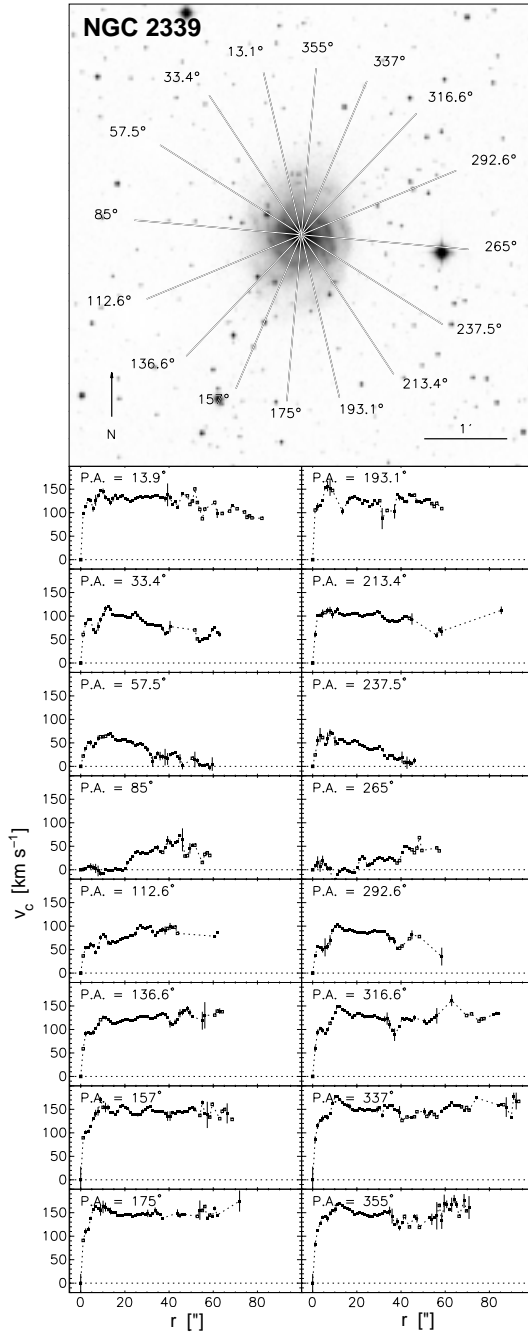


**Figure 3.2** NGC 2339

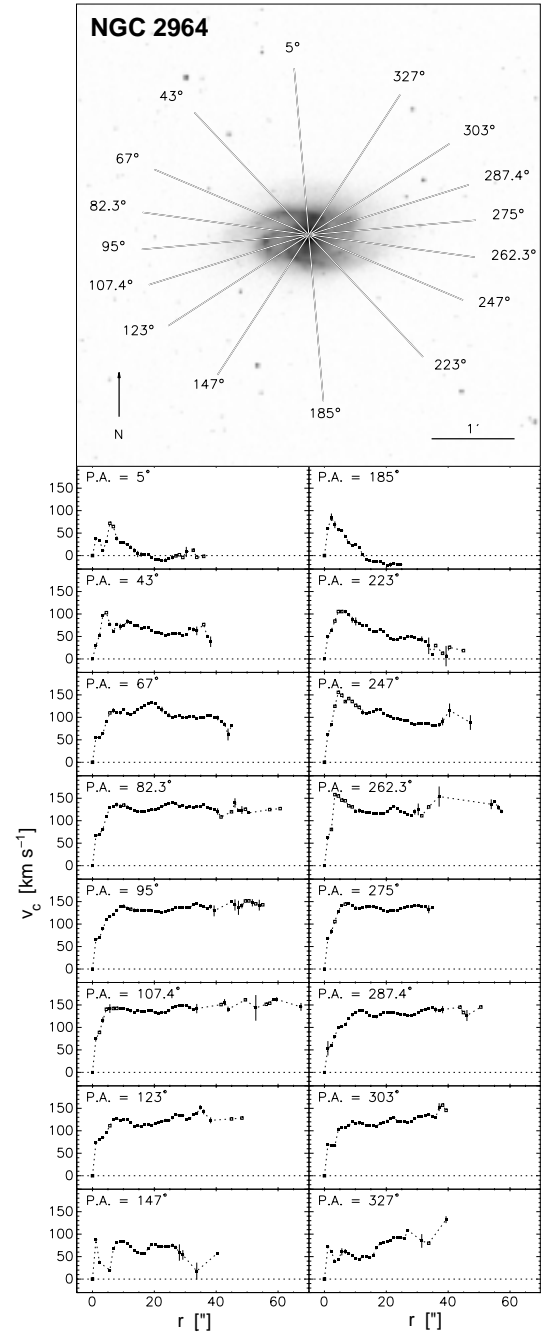


**Figure 3.2** continued. NGC 2964

Data for the subsample of galaxies with kinematic observations. The upper frame shows the  $K'$ -band image. The overlay shows the orientations of the spectrograph. In order to measure the 2D velocity field, ideally 8 longslit spectra were taken across the galaxies' disks (angles labelled in bold font) all crossing the nucleus. The measured rotation curves along the 16 slit positions are shown in the lower part of the Figure. Non-filled data points indicate errors larger than  $30 \text{ km s}^{-1}$ .

CHAPTER 3. OBSERVATIONS

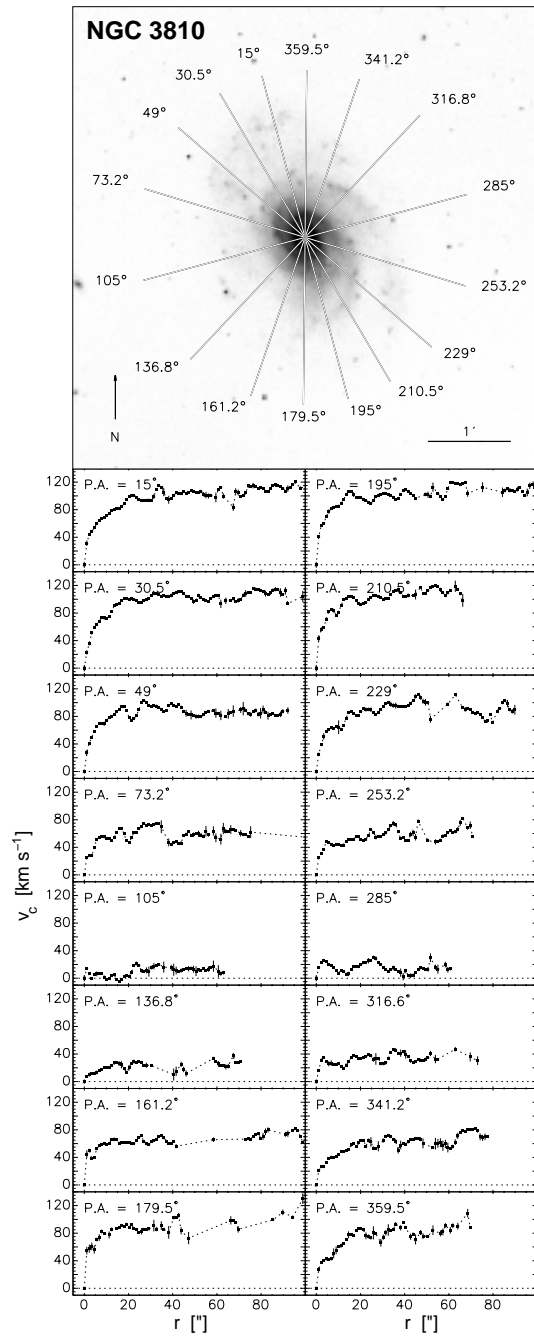


Figure 3.2 continued. NGC 3810

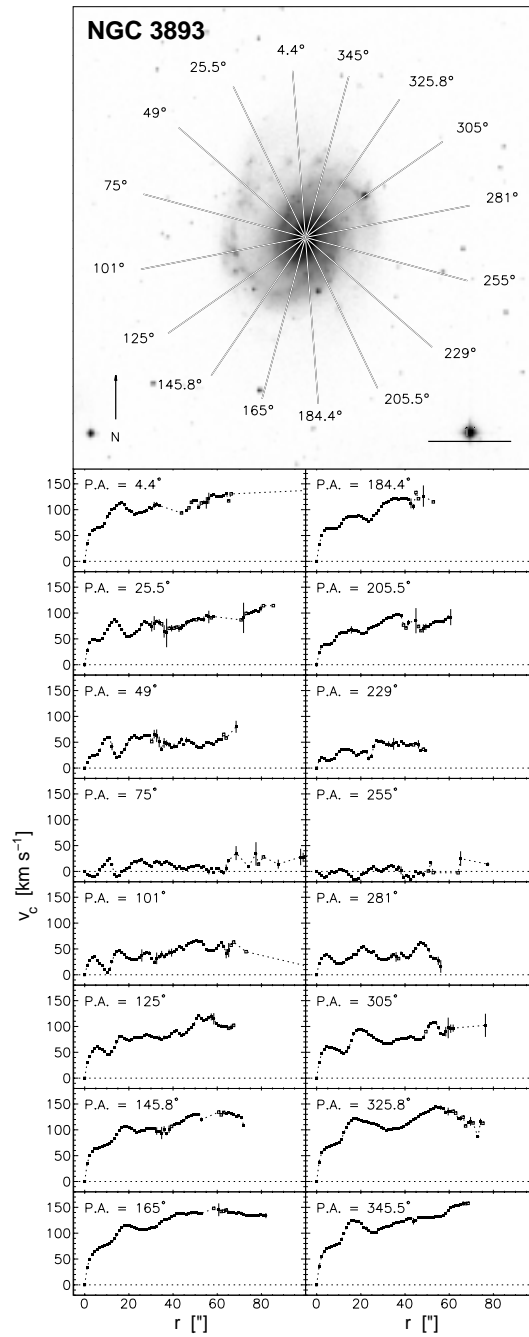


Figure 3.2 continued. NGC 3893

### 3.2. THE DATA

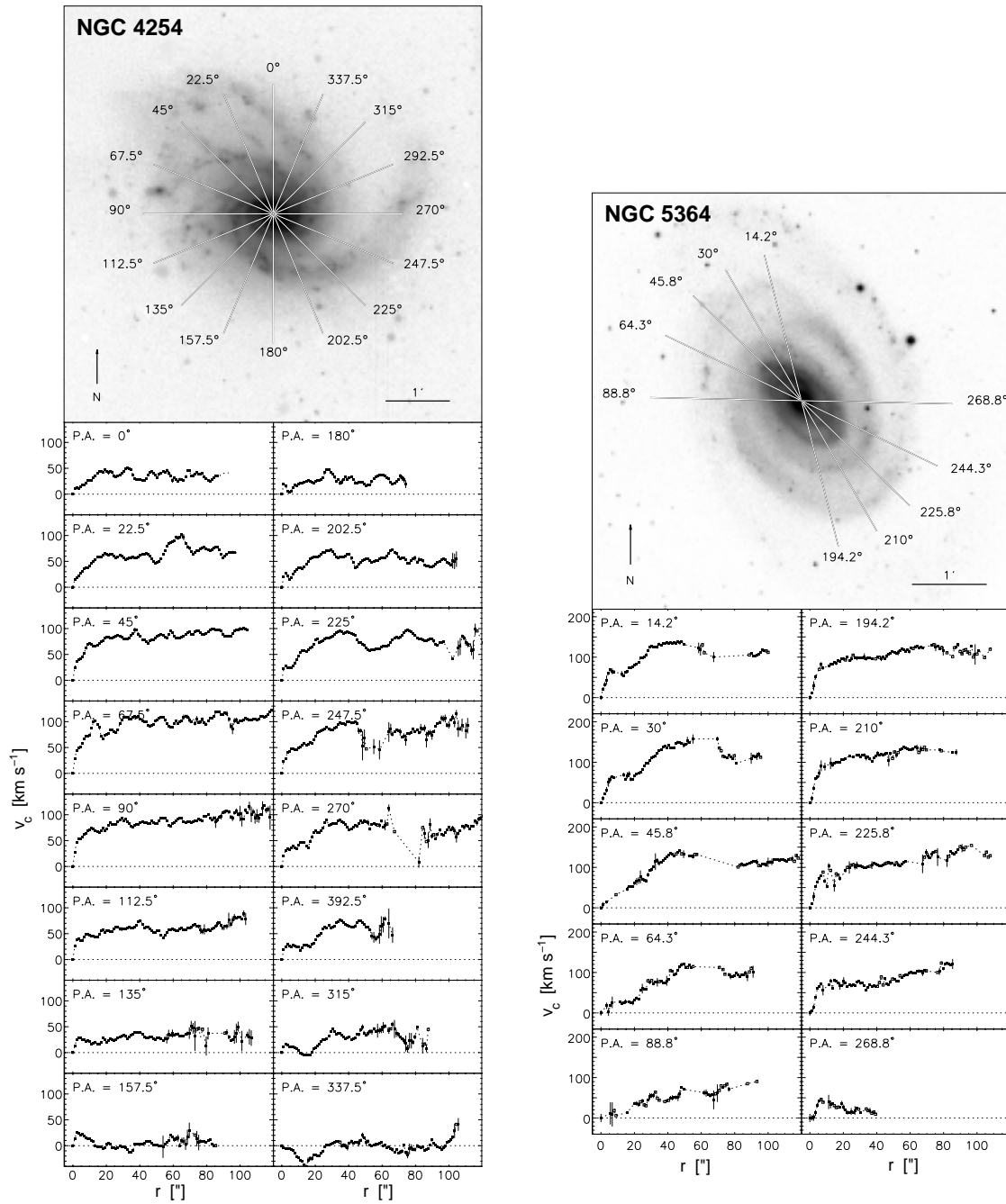


Figure 3.2 continued. NGC 4254

Figure 3.2 continued. NGC 5364, only 5 spectra could be taken.

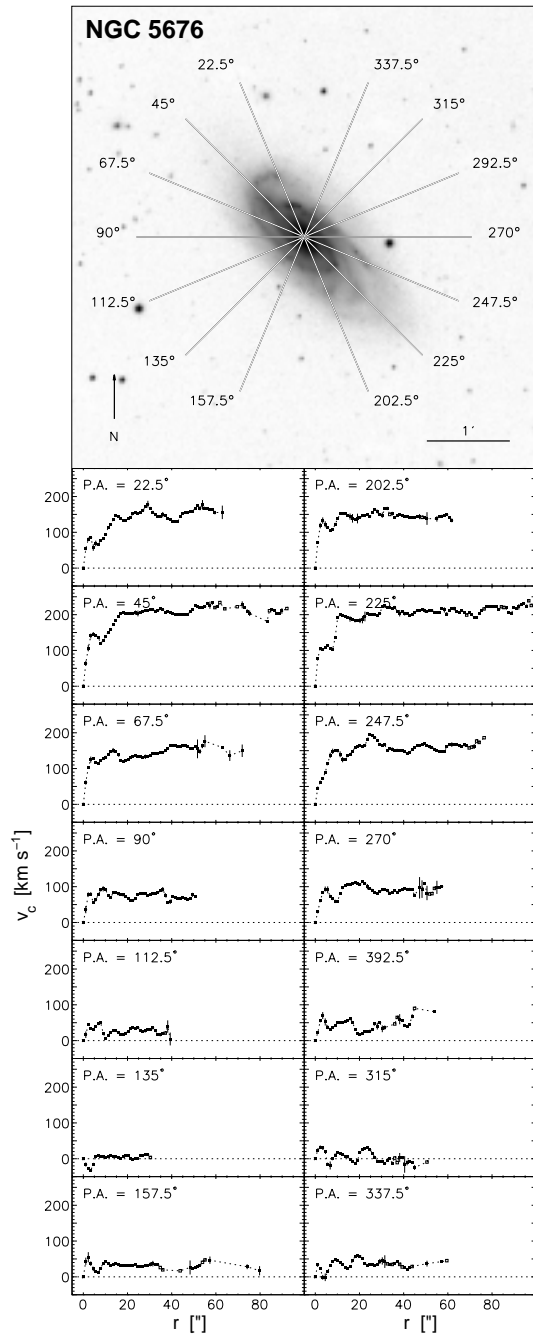


Figure 3.2 continued. NGC 5676, only 7 spectra could be taken.

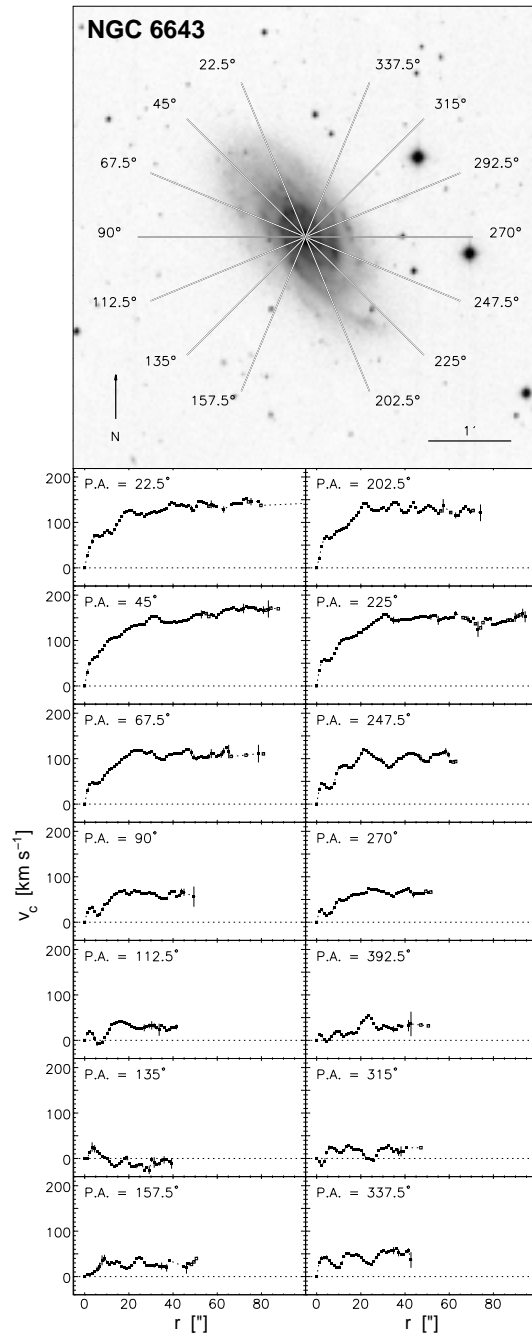


Figure 3.2 continued. NGC 6643, only 7 spectra could be taken.

### 3.3. Data reduction

#### 3.3.1. NIR photometry

For NIR detector arrays most of the calibration procedures, such as correcting for pixel to pixel gain variations or dark current subtraction, are very similar to those of optical CCD's. However, one basic difference is the sky brightness, which is outshining almost any astronomical object. During the Omega Prime runs, the sky brightness was in the range of 3500 counts per second per detector pixel, which translates to  $\approx 12 \text{ mag } \square''^{-1}$ . These conditions allowed only exposure times of 2 or 3 s, in order to not let the galaxy's nucleus reach the range where the chip shows deviations from linearity, which happens at  $\approx 25\,000$  counts. Furthermore, the sky brightness is highly variable and needs constant monitoring. In the end, the observing runs yielded as many sky background frames as science frames.

The actual measured detector voltage, or counts, contains several additional contributions besides the source flux. The main components that contribute to the measured voltage  $V(x, y)_m$  at each pixel for a measurement on target are:

$$V(x, y)_m = [G(x, y) \cdot (F(x, y)_g + F_s) + I_d] t \quad (3.1)$$

where  $G(x, y)$  is each pixel's photometric gain ( $e^-/\text{photon}$ ),  $F(x, y)_g$  is the extended source flux that should be isolated and  $F_s$  is the sky flux (photons/s),  $I_d$  is the dark current ( $e^-/\text{s}$ ) and  $t$  is the integration time. In principle  $F_s$  and  $I_d$  also exhibit pixel to pixel variations, but at first order both are approximately constant across the chip. The main components that contribute to the measured voltage  $V(x, y)_s$  at each pixel for a sky background measurement are as above:

$$V(x, y)_s = [G(x, y) \cdot (F_s) + I_d] t \quad (3.2)$$

The difference of the frame on target and the sky background frame eliminates all undesired effects except the pixel to pixel gain variation:

$$V(x, y)_m - V(x, y)_s = G(x, y) F_g t \quad (3.3)$$

The sky frames can also be used to correct for the chip's gain variations, since they exhibit only negligible flux variations across the field of view. Their use as "flatfield frames" is further motivated by their relatively high flux and the fact that numerous sky frames were taken. The sky frames are, however, not entirely free of sources. There are still stars in the field of view. The final flatfield frame used for data reduction was derived by calculating a median of a large set of scaled sky frames, to eliminate features from the background fields. Furthermore the dark current has to be subtracted from the sky flatfield frame. If  $N = F_s t$  is assumed to be a constant that normalizes the flatfield frame, from equation (3.2) it is found:

$$G(x, y) = (V(x, y)_s - I_d t) / N. \quad (3.4)$$

This procedure yields the source object's flux per unit time. To relate this quantity to astrophysical magnitudes, measurements of objects with known flux have to be evaluated.

For calibration purposes, several standard stars were observed repeatedly during the observations. The standard star measurements revealed only a very small variation of the zero point throughout the nights: in the three nights when most of the data were taken, the zero point variation was less than 0.095 mag, and even smaller in one single night ( $< 0.05$  mag). Figure 3.3 displays the standard star measurements for the night of March 17<sup>th</sup>, 2000.

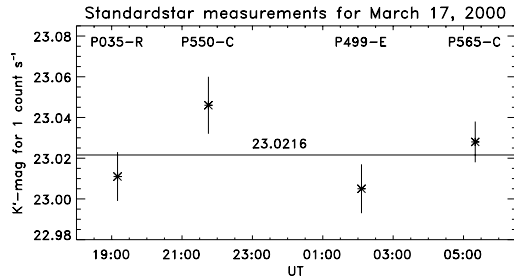


**Figure 3.3** Standardstar measurements in the night of March 17<sup>th</sup>, 2000. The four different stars (P035-R, P550-C, P499-E, P565-C) from the Persson et al. (1998) NIR standard star sample were observed during the night. The error bars refer to  $1\sigma$  errors.

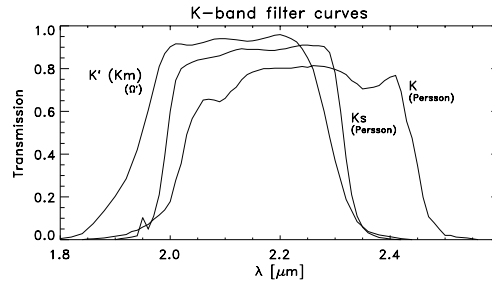


**Figure 3.4** Transmission curves of the  $K$ -band filters used for the observations ( $K'$  with Omega Prime) and the Persson et al. (1998) filters, for which the standard star fluxes are given.

A systematic error was introduced by the fact that the fluxes for the standard stars were only given for the  $K$  and  $K_s$  filters (Persson et al. 1998), whereas for the measurements the  $K'$  filter was used, whose filter curve differs slightly from both other filters (see Figure 3.4). However, the filter curves of the  $K'$  and  $K_s$  filter are very similar: about 93 % of the integrated area of the  $K_s$  filtercurve is inside that of the  $K'$  filter curve. Since the flux through the different  $K$  and  $K_s$  filters for the used subset of the Persson sample is compatible with being equal within their measured error bars and varies by maximally 0.02 mag, the expected difference between the  $K_s$  and  $K'$  filter would be even less. Thus, the Persson  $K_s$ -fluxes were used to calibrate the standard stars for the Omega Prime observations.

The data reduction was done using the ESO-MIDAS software package and self developed IDL routines. MIDAS was used for sky subtraction, flatfielding and for coaligning the dithered frames. For the sky subtraction sky frames were used that were interpolations of the sky frames taken before and after the object frame. The normalized flatfield frame was divided into the object frames. From all object frames a median image was computed to correct for strongly deviating pixels in the frames. Deviating pixels within single frames were then replaced by median values. The final image was derived from a mean of all preprocessed frames. The fine tuning of finding the zero-point of the sky background was done by looking at the radial light profiles of the disks. The sky background level was adjusted to not cause strong bends in the light profile while fading into the sky. Possible physical disk truncation effects were considered and an attempt was made to avoid them from being removed by adjusting the sky level. Finally, the images were cleaned from bright foreground stars. The magnitudes listed in Table 3.4 are given for the flux inside the 22  $K'$ -mag  $\square''^{-1}$  isophote.

### 3.3.2. H $\alpha$ kinematics

To extract the individual rotation curves from the raw data, the IRAF data reduction package, and again IDL routines were used. The IRAF package was used following the instructions given in Massey (1997) and Massey et al. (1992). The longslit spectra were reduced to a level that was required for extracting the rotation curves. Less priority was attributed to illumination corrections or flux calibration. The latter was not at all performed. To subtract the dark current from the frames and to flatfield the images with domeflat exposures the IRAF-tasks *zerocombine* and *flatcombine* were used in combination with the *ccdproc* task. The correction for distortions along the spatial axis of the longslit was a very important step to assure correct velocity measurements at all radii in the rotation curves. This correction procedure also included the wavelength solution for the spectra. The following tasks from the *noao/twodspec/longslit* package were used:

*identify* was used to identify the lines of the He-Ar lamp comparison spectrum along one dispersion line.

*reidentify* was then applied to re-identify these features at other ( $\approx 20$ ) dispersion lines along the spatial axis.

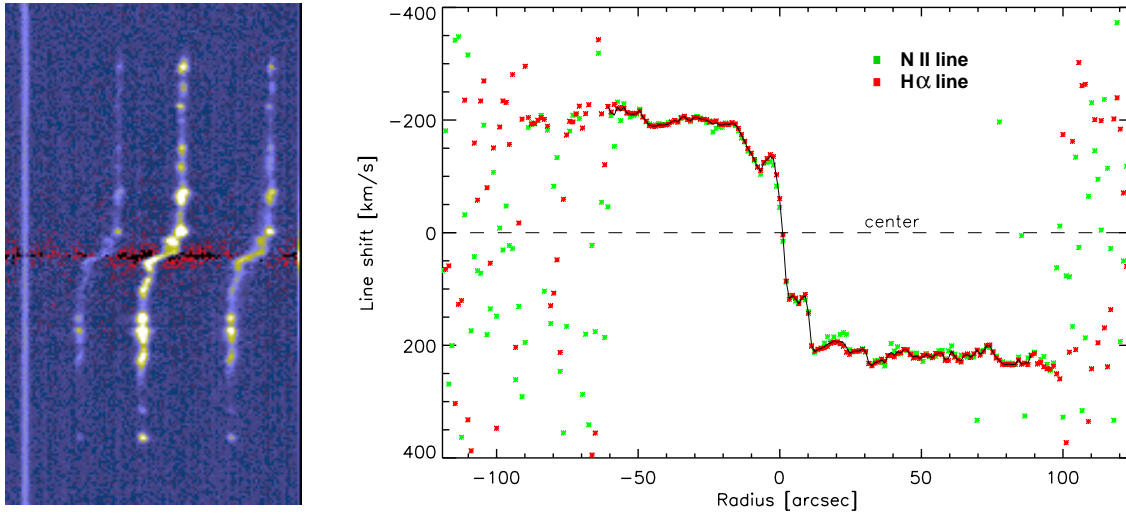
*fitcoords* then performs a fit of a two-dimensional function to the identified grid points all over the frame.

*transform* finally applies the geometrical correction to the original frame, correcting for the distortions along the spatial axis and giving the log of the wavelength as a linear function along the dispersion axis.

Residual distortions can be mapped from night sky lines and get accounted for when determining the line centers.

The further data reduction was done using self developed IDL routines. In a first step the cosmic rays were removed from the relevant parts of the spectra by replacing the spikes with adjacent pixel values. This process was kept interactive to assure the quality of the correction. After removal of (all but one) night sky lines and the galaxy's continuum emission, the rotation curves could be measured. The line-of-sight (LOS) velocity component of the ionized gas was determined as a function of radius from the galactic center from Doppler shifts of the H $\alpha$ -line and the brighter N II-line at 6584 Å (the right emission line in Figure 3.5). The central values for the LOS velocity of the emission lines were determined by fitting a single Gaussian profile to the observed line profile. The single Gaussian appeared to be a good enough description of the real line profiles to determine the line centers to sub-pixel resolution. The final rotation curve was calculated from the 3:1 weighted coaddition of the two fits (see Figure 3.5). The weights were derived from the relative line strengths. The comparison of the two fits yielded the uncertainty of the line center position, which was taken as  $\sigma = \sqrt{0.75(\text{H}\alpha - \text{mean})^2 + 0.25(\text{NII} - \text{mean})^2}$ . Residual slit distortions along the spatial axis were corrected by fitting a low order polynomial to spatial distribution the night sky line center and subtracting the deviations of the polynomial from its mean from the rotation curve.

The final step was to find the zero-point of the spectra, defining the dynamic center of the disk. As it was apparent from the spectra, the dynamic center didn't always coincide with

NGC 5676 – H $\alpha$  and NII lines at 45° position angle


**Figure 3.5** Data example for NGC 5676. Shown is the spectrum from slit position 45°, which is very close to the major axis position angle. At left the fully reduced TWIN spectrum is shown for the wavelength region of the H $\alpha$ -line and the two NII-lines for a width of 68 Å. One night sky line (left in the image) had not been removed to check for residual distortions along the spatial axis. At right, the derived line shifts are plotted. The green data points refer to the line shifts determined from the NII-line (the right one in the image at left), while the red data points refer to the H $\alpha$ -line. The line shift has been translated into line-of-sight velocities. The continuous black line is the weighted average rotation curve

the light center of the continuum emission. In these cases the zero-point was determined such that the asymptotic rotation curves reached about the same velocity on both sides of the galaxy. Systematic errors arising from all these procedures were accounted for by adding an overall systematic error to all rotation curves when comparing with the results from the simulations.

The line shifts were translated into LOS rotation velocities making use of

$$dv = c \frac{d\lambda}{\lambda} = c d \ln \lambda = c 2.3026 d \log \lambda \quad (3.5)$$

where  $d \log \lambda$  is the line shift in the wavelength calibrated spectrum. The per pixel resolution is  $3.596 \times 10^{-5}$  for the TWIN spectrograph, corresponding to  $24.8 \text{ km s}^{-1}$ .

### 3.4. Derived quantities

For this discussion, the focus will be on the NIR properties of the galactic disks. A first step to analyze the light distribution is to find the inclination and position angles of the galaxies and to perform the deprojection of the disks. In cases where there is only NIR photometry available, the inclinations and position angles were estimated by approximating an ellipse to the faintest isophotes of the galaxy. The precision with which the values can be determined from this method depends on the inclination of the particular galaxy.

### 3.4. DERIVED QUANTITIES

Best results were obtained for  $i \approx 60^\circ$ . An average uncertainty of  $\sim 3^\circ$  must be attributed to all values. The inclinations and position angles of these galaxies, for which observed gas kinematics is available, could be determined quite reliably from the spectra. They were derived from a global  $\chi^2$ -fit of an axisymmetric rotation curve model to the 16 observed rotation curves. The model was based on a combination of stellar and dark halo rotation curves which were scaled to an average rotation curve from the six slit positions closest to the major axis (as shown in Figure 3.7). The uncertainty range for the kinematic fitting method is less than  $1^\circ$ . However, for NGC 4254 it has been found during the modelling procedure that it might matter whether an axisymmetric rotation curve model is used for the fit or a 2D velocity field from a hydrodynamical gas simulation. In most cases those different methods lead to very similar results. Only for NGC 4321 literature values had to be adopted since this galaxy's size on the sky is larger than the field-of-view of the Omega Prime camera. A reliable estimate from the data was not possible. The derived parameters for the sample galaxies are compiled in Table 3.4.

**Table 3.4** Derived parameters from the NIR photometry.

Galaxy	P.A. [ $^\circ$ ]	incl [ $^\circ$ ]	Method (see Note)	$K'_{\text{tot}}$ < 22 mag $\square''^{-1}$ [mag]	central surface brightness	
					bulge [mag $\square''^{-1}$ ]	disk [mag $\square''^{-1}$ ]
NGC 2336	0.0	59.0	E	7.83	14.93	18.12
NGC 2339	175.0	41.4	K	8.53	12.78	16.68
NGC 2964	95.0	56.0	K	8.44	13.95	16.98
NGC 2985	175.0	41.4	E	7.51	13.24	15.89
NGC 3583	123.0	53.1	E	8.51	13.95	16.56
NGC 3810	22.0	46.0	K	8.02	14.46	16.21
NGC 3893	166.0	42.0	K	7.94	14.80	16.74
NGC 3953	10.0	60.8	E	7.37	14.58	17.70
NGC 4254	67.5	41.2	K	6.85	14.83	16.78
NGC 4321	32.0	30.0	L	6.60	14.15	17.59
NGC 4535	0.0	44.0	E	7.31	13.87	17.98
NGC 4653	26.0	32.2	E	9.86	17.02	18.19
NGC 5248	135.0	54.5	E	7.32	14.37	17.22
NGC 5364	30.0	46.6	K	7.62	16.26	18.32
NGC 5371	7.0	38.2	E	7.66	16.54	17.44
NGC 5676	46.5	63.2	K	8.03	14.97	16.79
NGC 5985	13.0	60.9	E	8.13	15.77	17.89
NGC 6118	55.0	67.8	E	8.32	16.97	18.58
NGC 6643	39.0	57.5	K	8.18	15.64	17.19

Note: The abbreviations for the method of determining the galaxy's position angles and inclinations stand for the following: E = from ellipse fitting; K = from gas kinetic measurements; L = from the literature.

Having determined the projection angles of the galaxies, the IDL routine 'GAL\_FLAT' from the astrolib was used to deproject the galaxy images to face-on (the deprojection process will be described in more detail in Section 4.1.3). These deprojected frames were then

## CHAPTER 3. OBSERVATIONS

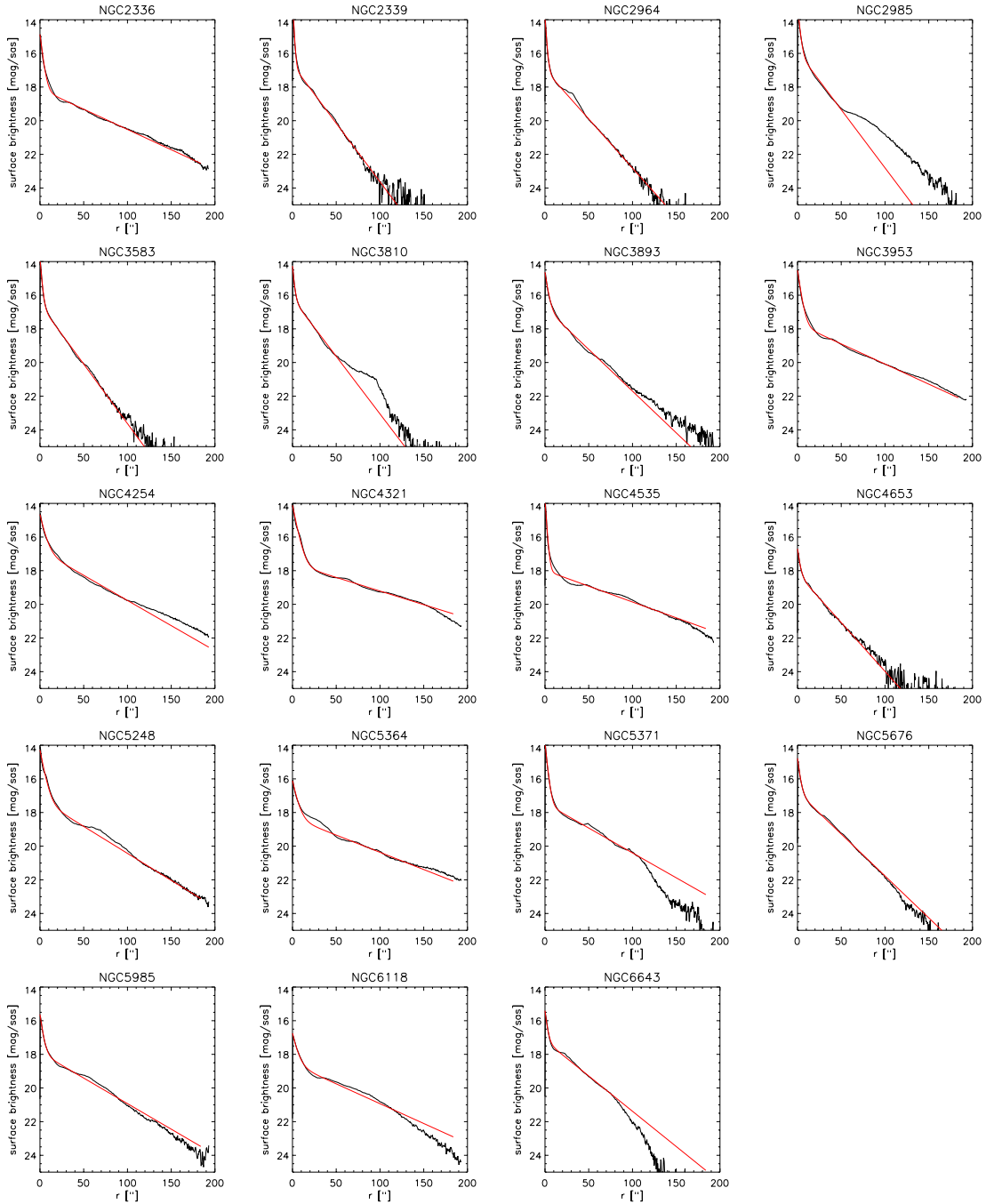


**Figure 3.6** Radial light profiles in  $K'$  for all galaxies from the sample. For most galaxies the  $K$ -band light is well approximated by a double exponential profile, given by the red line.

used to find the averaged radial  $K$ -band light profile and the disk scale lengths. Since the sample consisted of late type spirals with small bulges, for most of the galaxies a double exponential bulge/disk model provides a very good fit to the radial  $K$ -band light profile as shown in Figure 3.6. The parameters that were derived from the photometry are given in

### 3.4. DERIVED QUANTITIES

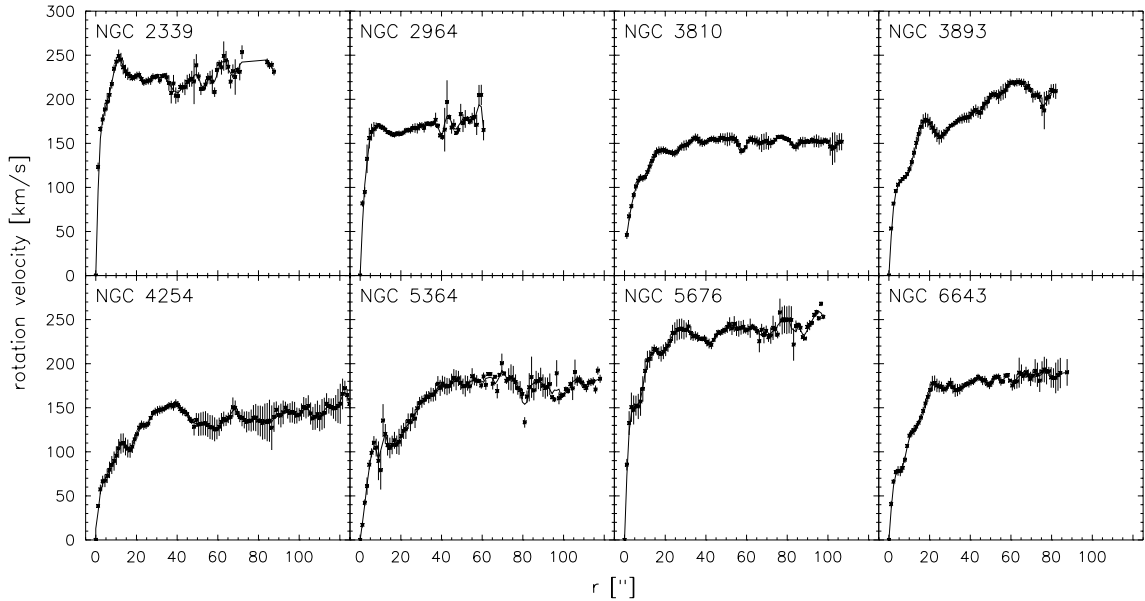


**Figure 3.7** Averaged rotation curves of the sample galaxies. Each  $H\alpha$  rotation curve shown above is an average of rotation curves from six spectrograph slit positions that were oriented closest to the major axis position angle. The rotation curves are inclination-corrected and render intrinsic velocities.

Table 3.4. It shows that the sample comprises mainly of high surface brightness galaxies which have a central disk surface brightness of  $\approx 17 \text{ mag } \square''^{-2}$  in  $K'$ .

Figure 3.7 shows the rotation curves that were derived from the  $H\alpha$ -longslit spectra. The presented rotation curves are averages of spectra taken at those six slit position angles that were taken closest to the major axis position angle. The rotation curves are presented to show intrinsic velocities, i.e. projection effects were taken into account and were corrected according to the parameters given in Table 3.4.

#### 3.4.1. Remarks to individual galaxies

For the galaxies for which both photometric and kinematic data are available, a few remarks about their morphology and environment are given. More detailed information will be provided in Chapter 5 and Chapter 6, where the modelling of individual objects is being discussed.

**NGC 2339** exhibits a small, very bright nucleus in a weak complex bar. In the  $K$ -band there are faint arms, revealing an inner 3-arm morphology. It is a bright IRAS source.

**NGC 2964** is a starburst galaxy that exhibits strong star formation activity across the whole disk and the nucleus. It does not exhibit a clear grand design spiral structure, although there is a prominent arm-structure in the disk. NGC 2964 is a non-interacting pair with NGC 2968 at  $5.8$  projected distance.

**NGC 3810** is a Sc galaxy in the Leo group. In the central parts ( $< 45''$ ) NGC 3810 looks like a grand design spiral but further out the arms become more flocculent. There

are no closeby galaxies interacting with NGC 3810. The radial profile of the outer disk deviates considerably from exponential and beyond  $100''$  the disk appears to be truncated.

**NGC 3893** is a grand design Sc galaxy in the Ursa Major Cluster of Galaxies. In the outer parts the symmetry of the spiral is disturbed by interaction with its companion NGC 3896 located  $3.9'$  to the south-east. There is enhanced star formation activity in the interacting arm as compared to the arm at the opposite side.

**NGC 4254** is a bright Sc galaxy, located in the Virgo galaxy cluster. It exhibits a lopsided three-arm morphology, that is seen much stronger in the optical than in the NIR. The south-western arm is more pronounced than the others. There is vigorous star forming going on along the spiral arms. Although there is no major galaxy in the immediate vicinity, it has been found that NGC 4254 interacts with the gaseous medium of the cluster (Phookun et al. 1993). It appears to have a weak bar at a position angle of  $\sim 45^\circ$ .

**NGC 5364** is an extremely regular galaxy whose spiral arms can be clearly traced for more than  $400^\circ$ . They emerge from an inner ring that is completely closed. Inside this ring there is a nuclear spiral winding in the same sense. It has been argued (Braine et al. 1993) that this galaxy might be disturbed because the spiral arms wind "too much" and there are several galaxies very nearby.

**NGC 5676** is a starburst galaxy with a fairly regular grand design structure. There are many bright, knotty star forming regions and filamentary arms overimposed. It has several sudden changes in the spiral's pitch angle.

**NGC 6643** is – like NGC 5676 – a starburst galaxy with a fairly regular grand design structure. It exhibits a considerable lopsided morphology with a third arm and filamentary arms at the outer regions. There is no evidence for interaction.